Electrical Power and Energy Systems 149 (2023) 109010

Contents lists available at ScienceDirect

International Journal of Electrical Power and Energy Systems

journal homepage: www.elsevier.com/locate/ijepes

Power oscillation damping method suitable for network reconfigurations based on converter interfaced generation and combined use of active and reactive powers☆

Njegos Jankovic [a,*], Javier Roldan-Perez [a], Milan Prodanovic [a], Jon Are Suul [b], Salvatore D'Arco [b], Luis Rouco Rodriguez [c]

[a] Electrical Systems Unit, Imdea Energy, Av. Ramon de La Sagra, 3, Mostoles, 28935, Spain
[b] Energy Systems, SINTEF Energy, Strindvegen 4, Trondheim, 7010, Norway
[c] Instituto de Investigacion Tecnologica, Icai Universidad Pontificia Comillas, Calle de Alberto Aguilera, 25, Madrid, 28015, Spain

ARTICLE INFO

Keywords:
Power oscillation damping
Low-frequency oscillations
Power modulation
Network reconfiguration
Power oscillation damping controller

ABSTRACT

Power system stabilisers (PSSs) are commonly used in synchronous generators for damping low-frequency oscillations. However, many of these machines have been replaced by converter-interfaced generators (CIGs), such as those used in solar power plants. This means that CIG-based power plants should also contribute to oscillation damping. Moreover, CIGs may use both active and reactive power for power oscillation damping (POD). However, their combined use has been seldom studied in the literature. Moreover, only a few articles have addressed the adaption of POD controllers when the power system changes (e.g., after a fault). In this paper, a POD controller for CIG-based power plants is proposed that is suitable for operation in power systems exposed to reconfiguration. This controller takes advantage of both active and reactive power injection to maximise the damping of the power system. This controller is based only on local measurements so communication systems are not required. Theoretical developments were validated in a laboratory using real power converters including a 75 kVA grid emulator where the two-area benchmark model is emulated and four 15 kVA CIGs operating in parallel connection. The applicability of the proposed controller was also explored for the IEEE 39-bus system.

1. Introduction

Low-frequency oscillations are an inherent phenomena in electrical networks with interconnected synchronous generators (SGs). These oscillations appear as a result of interactions between generators (or groups of them), with their frequency and magnitude determined by the SGs parameters, their control loops and the power system topology [1]. Commonly, the SG control system includes an additional control loop called power system stabiliser (PSS) that is designed to damp low-frequency oscillations [2]. However, the massive integration of renewable energy sources results in SGs being replaced by converter interfaced generators (CIGs) [3]. In their basic configuration, CIGs are controlled as power sources that extract the maximum power from the renewable sources and, therefore, they do not offer ancillary services such as power oscillation damping (POD). This operating mode was adequate for the relatively small share of renewable energy sources in the system. However, as the number of these sources is rapidly increasing, new regulations requesting CIG-based power plants to have POD capabilities are imposed [4].

Some early ideas for damping oscillations using CIGs were introduced in the 80's. In [5] the operation of conventional PSS control was replicated by the control system of wind turbines. Structure similar to the PSS is applied to photovoltaic (PV) [6] and more advanced wind power plants [7]. In these cases, the damping action is achieved by using only active power. Therefore, the damping action effectiveness is linked with the designated amount of active power. However, this has an economical impact since the power delivered to the network is below maximum point during the steady-state operation. The most feasible solution that was recently presented allocates the power for

☆ This work has been financed by the following research projects: PROMINT Ref: P2018/EMT4366 is funded by Regional Government of Madrid, Spain. DRES2MARKET Grant Agreement 952851 is funded by European Commission. Juan de la Cierva Incorporación program (IJC2019-042342-I) is funded by Spanish Ministry of Science and Innovation.

* Corresponding author.
E-mail address: njegos.jankovic@imdea.org (N. Jankovic).

https://doi.org/10.1016/j.ijepes.2023.109010
Received 19 September 2022; Received in revised form 14 December 2022; Accepted 27 January 2023
Available online 16 February 2023

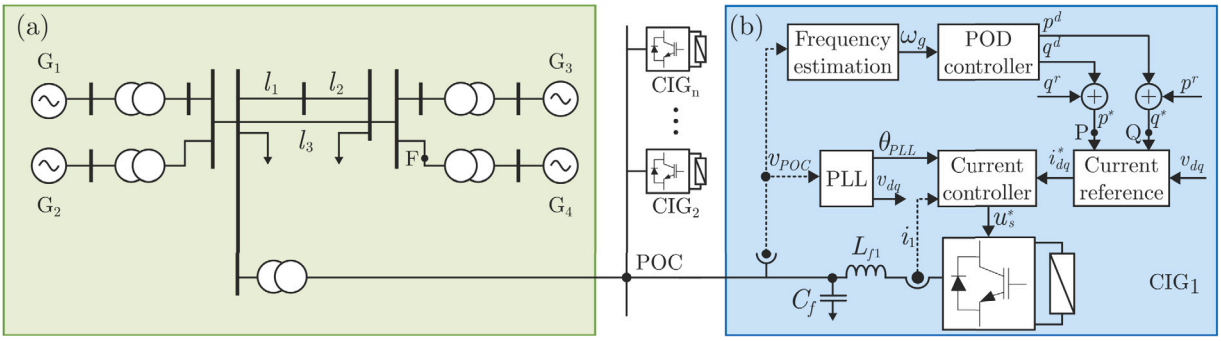

Fig. 1. Single-line diagram of the network studied in this article and the CIG control system. It consists of a power plant with n CIGs.

POD dynamically when the oscillation starts [8]. This improves the feasibility, however, the active power injection is likely to be reduced during oscillatory events that may create additional frequency issues in addition to those that triggered the low-frequency oscillation.

Another approach to oscillations damping is to inject both active and reactive power [9,10]. This option is of interest for power plants based on CIGs since reactive power is less restricted provided that the ratings of power conversion stages are not surpassed. This approach has been applied in recent years and it has shown that the damping capability of the power plant increases [11–13]. These solutions show that by introducing the reactive power damping action, the system stability margins improve significantly. However, negative interaction between two control loops can occur. Namely, Rimorov et al. [14] addressed this issue showing that the interaction between control loops in active and reactive powers can deteriorate the damping performance. Thus, the authors propose the coordinated design of POD controllers in both loops. However, the proposed procedure requires an optimisation algorithm to be run. Moreover, the effect of the system topology reconfiguration (e.g., due to faults, disconnections, etc.) was not explored, yet it is known electrical networks are prone to changes in their topology and, consequently, in their dynamics. As POD controllers are designed for the system with certain grid topology, these changes may lessen the overall system damping.

Wide-Area Measurement Systems (WAMS) are used for exchanging information regarding the system topology [15], and this information can be used then to recalculate the controller parameters online [16] or by using a predefined bank of controllers [17]. The system would be, therefore, maintained well-damped even if the system topology changes [18]. However, these strategies rely on communication systems, adding a significant complexity to the system and jeopardising its reliability. This is a critical issue for POD controllers since they act instantaneously in the presence of an oscillation. Moreover, the event that triggers the oscillation (e.g., the disconnection of a line) might cause a system reconfiguration. This means that POD controllers would require retuning and centralised controllers would require extra time to react in this situation. Due to the aforementioned reasons, POD controllers based on local measurements are considered to be more robust.

Non-adaptive POD controllers are commonly used to damp oscillations and some works propose adaptation mechanisms for them [19,20]. For example, Beza et al. [21] use recursive least squares to adjust the parameters of POD controllers if changes in the network are detected. In [22], the parameters are updated based on demand predictions using an additional neural network. Other methods such are fuzzy logic [23] and Kalman filter [24] have also been explored. In this case, the update of the controller parameters improved the damping action under different operating conditions. In summary, these alternative options provide adequate damping of oscillations. However, they are quite complex and require knowledge of advanced engineering tools (e.g., artificial intelligence techniques). Moreover, their implementation at the device level would require important engineering efforts. For that reason, the development of adaptive POD strategies suitable for implementation at the device level is of interest.

In this paper, a POD controller for CIG-based power plants is proposed. This controller takes advantage of active and reactive power injection capability of the power plant and it is adapted whenever a change in the electrical system topology is detected. These changes are detected by observing the frequency of the oscillation. It is first shown that most common grid topology modifications (e.g., disconnection of a line and variation in the equivalent system inertia) are directly linked to the frequency of the oscillation. The link between the oscillation frequency and the parameters of the POD controller is extracted via an off-line analysis and then used for the real-time operation. The adjustment of the POD controller parameters following the established relationship significantly improves the system damping when the change in the network topology occurs. The fundamental developments of the work are validated by using both theoretical analysis and a laboratory set-up comprising four 15 kVA power converters operating as CIGs. The dynamics of the electrical system are emulated by using a 75 kVA grid emulator running a benchmark model that is typically used for inter-area oscillation studies [1]. Furthermore, an off-line analysis is conducted for the IEEE 39-Bus network, A similar link between the oscillation frequency and the phase to be compensated is established.

2. System overview and methodology

2.1. System description

Fig. 1 shows the electrical and control system diagrams of the network studied in this work. It can be divided into two main parts. The first part is depicted in Fig. 1(a) and represents a model of a transmission network formed by four generation units (G_1 to G_4). This model is widely used as a benchmark for inter-area oscillation studies [1]. Each generation unit includes a synchronous generator with a governor and an exciter. The unit $G2$ includes a PSS. With this configuration the system is stable, but it has a poorly damped inter-area oscillation. In the left part of Fig. 1, an additional power plant has been connected to the area formed by G_1 and G_2 via the point of connection (POC). It consists of n CIGs in parallel connection that have the identical electrical elements and control systems.

Fig. 1(b) shows the power stage and control system of one CIG. The power stage consists of a primary energy source on the dc side, a three-phase voltage source converter (VSC) and an LC filter. The CIG control system includes inner and outer control loops. The inner control loop regulates the VSC output current (i_1). This controller is implemented in a synchronous reference frame (SRF) and includes two proportional–integral (PI) controllers and a phase-locked loop (PLL) synchronised with the POC voltage (v_{POC}). The outer control loop calculates the current reference for the inner control loops by using the established technique shown in [25]. The active and reactive power references (p^* and q^*) consist of two terms. The first one is sent by the grid operator

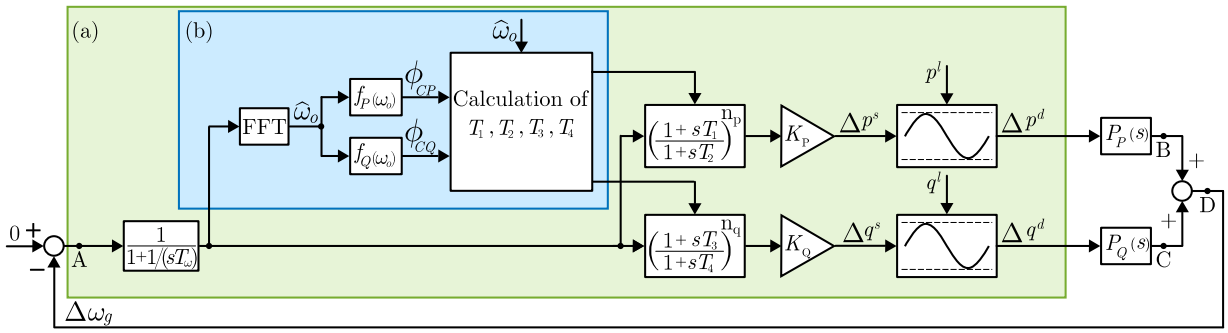

Fig. 2. POD controller block diagram, including the dynamics of the plants.

or generated internally (superscript "r"), while the second adds an oscillatory component that is used to damp oscillations (superscript "d"). A frequency estimator is used to estimate the POC frequency ($\hat{\omega}_g$). The frequency estimator is introduced, although the POC frequency can be obtained from the PLL. This is done to avoid any type of coupling between the dynamics of the PLLs [26]. Finally, the POD controller calculates p^s and q^s according to $\hat{\omega}_g$.

2.2. POD controller overview

Fig. 2 shows the block diagram of the POD controller proposed in this work and the transfer functions that link active and reactive power with the estimated network frequency ($P_P(s)$ and $P_Q(s)$, respectively). The POD controller can be divided in two parts. The first part is depicted in Fig. 2(a) and includes the controllers for both active and reactive power. The high-pass filter eliminates the steady-state value from the estimated frequency so that the POD controller acts only at the oscillatory frequency. Then, the lead–lag compensators (to be called $C_P(s)$ and $C_Q(s)$) generate the power references (p^s and q^s) to compensate the open-loop phase of the plant and then maximise the damping effect. The POD controller also includes proportional gains (K_P and K_Q) and saturators.

2.3. Real-time adaptation of POD controllers

Fig. 2(b) shows the part of the POD controller in which the phases to be compensated by the lead–lag compensators are calculated. First, an algorithm based on the fast Fourier transform (FFT) is applied to the estimated POC frequency in order to determine the frequency of the oscillation (ω_o). Then, the phases to be compensated (ϕ_{CP} and ϕ_{CQ}) are calculated using the predefined functions $f_P(\omega_o)$ and $f_Q(\omega_o)$. These functions are obtained using offline simulations, in which the network model is examined under different operating conditions in order to find the relationships between ω_o, ϕ_{CP} and ϕ_{CQ}. It is worth noting that the relation between ω_o and the compensation phases is not unique nor perfectly defined since it depends on several variables of the electrical system. However, it will be shown that these variables are clearly linked, and basic adaptation rules (e.g., a linear relationship) will greatly improve the effectiveness of POD. The development, analysis and implementation of this technique represent the main contribution of this work.

2.4. POD controller design methodology

Fig. 3 shows the main steps used to design and operate the proposed controller. The procedure can be divided into two parts. The first one is shown in Fig. 3(a) and represents the offline analysis of the power system. The main goal is to determine the phases to be compensated by the POD controllers according to the network topology. First, the possible alternative network reconfiguration are identified (faults, disconnections, etc.). A subset of variations in which the system remains

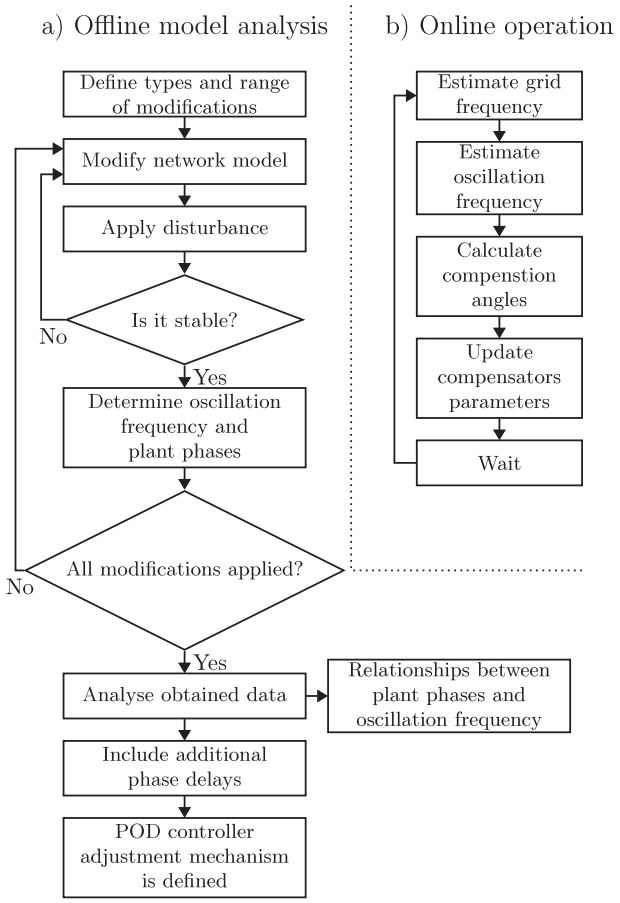

Fig. 3. Procedure for the design and operation of the POD controller. (a) Offline model analysis and (b) online operation.

stable is selected. In the case of an unstable system, time-domain simulation results would not be reliable. Then, for each configuration, the system oscillation frequency (ω_o) is calculated using simulation. Once this frequency is known, the phases to be compensated (ϕ_{PP} and ϕ_{PQ}) are calculated. This process is repeated for all network configurations considered. With the data for all the cases obtained, the challenge is to find the relationships between ω_o, ϕ_{PP} and ϕ_{PQ}. Then the functions $\phi_{PP} = f_P(\omega_o)$ and $\phi_{PQ} = f_Q(\omega_o)$ are fitted.

The online operation of the POD controller is depicted in Fig. 3(b). First, the grid frequency is estimated from the POC voltage measurements. This signal is analysed and the oscillation frequency (ω_o) extracted by using a FFT algorithm. After ω_o is estimated (called $\hat{\omega}_o$), it is inserted in the previously calculated functions $\phi_{PP} = f_P(\omega_o)$ and $\phi_{PQ} = f_Q(\omega_o)$. Finally, the lead–lag compensators are adjusted to

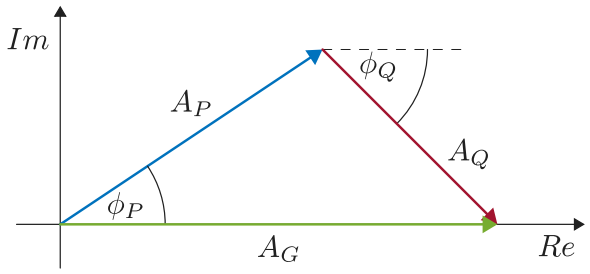

Fig. 4. Vector diagram representation of $G(j\omega_o)$.

compensate these phases. In this paper, the analysis is carried out in a simulation model implemented in MATLAB/SimPowerSystems [27], following acausal modelling principle. However, the same analysis can be carried out from the small-signal model. This procedure is repeated after a certain period of time. It can be seen that the tools used for the real-time implementation are readily available in microprocessors that are commonly used to control CIGs. Therefore, this strategy is suitable for the implementation on standard converter controller platforms.

3. POD controller design

In this section, the POD controller design objective is defined. It helps to understand how active and reactive powers affect the system damping. Finally, active and reactive power limits are discussed.

3.1. Design objective

The design objective is to maximise the damping effect of the CIG at ω_o. To formulate this objective using a standard notation, the open-loop ($G(s)$) and closed-loop ($F(s)$) transfer functions are defined [28]. From Fig. 2:

$$F(s) = G(s)/(1 + G(s)), \tag{1}$$

where $G(s)$ is the transfer function from point A to point D in Fig. 2. As the signals involved would be of a specific frequency (ω_o), the design criteria selected is to maximise the closed-loop gain at ω_o. This can be written as:

$$\max|F(j\omega_o)| = \max|G(j\omega_o)/(1 + G(j\omega_o))|, \tag{2}$$

where

$$G(j\omega_o) = A_G e^{j\phi_G}. \tag{3}$$

Condition (2) can be simplified as follows:

$$\max|F(j\omega_o)| = \max A_G/|1 + A_G e^{j\phi_G}|. \tag{4}$$

The value of A_G is the system gain so it is considered as constant (in real applications, it will be limited by practical design criteria). Then, it is clear that the maximum value in (4) is obtained for $\phi_G = 0$. This means that the lead–lag compensator must compensate all the phase introduced by the rest of the elements at ω_o. This criteria does not actually guarantee the maximum damping for the closed-loop eigenvalues of the system. However, it greatly improves the system damping with a clear physical meaning, so it is commonly used in the literature [1]. Furthermore, for the system with several modes with the same frequency, the criteria defined in (4) would contribute to the overall damping of those modes. On the other hand, if the system has several poorly damped modes in the low-frequency range, the criteria from (4) needs to be extended. This is of interest for future work.

3.2. Controller definitions

The open-loop transfer function includes the active and reactive power action, and it is defined as:

$$G(s) = G_P(s) + G_Q(s), \tag{5}$$

where

$$G_P(s) = H(s)K_P C_P(s)P_P(s), \tag{6}$$

$$G_Q(s) = H(s)K_Q C_Q(s)P_Q(s). \tag{7}$$

The transfer functions $G_P(s)$ and $G_Q(s)$ represent the relation between the active and the reactive power injections, and the frequency (in Fig. 2, from point A to B, and from point A to C, respectively). From now on, subscript P refers to active power while subscript Q refers to reactive power, $C(s)$ means phase compensator and $P(s)$ means plant. The transfer function $H(s)$ represents a high-pass filter.

The lead–lag compensators are defined as:

$$C_P(s) = \left(\frac{1 + sT_1}{1 + sT_2}\right)^{n_p}, \tag{8}$$

$$C_Q(s) = \left(\frac{1 + sT_3}{1 + sT_4}\right)^{n_q}, \tag{9}$$

where T_{1-4} are time constants, and n_p and n_q represent the number of compensators.

The high-pass filter is defined as:

$$H(s) = 1/(1 + 1/(sT_\omega)), \tag{10}$$

where T_ω is used to control the filter bandwidth.

3.3. Lead–lag controller design

The lead–lag compensator is designed to adjust the phase ϕ_G, which can be calculated as follows:

$$\underbrace{A_G e^{j\phi_G}}_{G(j\omega_o)} = \underbrace{A_P e^{j\phi_P}}_{G_P(j\omega_o)} + \underbrace{A_Q e^{j\phi_Q}}_{G_Q(j\omega_o)}, \tag{11}$$

where A will be used from now on to represent the magnitude of a complex number, while ϕ will represent its phase. Fig. 4 shows a graphical representation of (11) in the form of a vector diagram. It can be seen that the design criteria $\phi_G = 0$ can be met by choosing any combination of $G_P(j\omega_o)$ and $G_Q(j\omega_o)$ that results in $\mathrm{Im}\{G(j\omega_o)\} = 0$. However, from Fig. 4, it is clear that for a fixed value of A_G, $|F(j\omega_o)|$ is maximised if:

$$\phi_G = \phi_P = \phi_Q = 0. \tag{12}$$

This mathematical condition yields a result that is evident: the active (reactive) power controller should compensate for the phase of the active (reactive) power plant. Furthermore, it means that the controllers in the active and reactive power loops are designed independently. Nonetheless, the positive combined control action of both controllers relays on the superposition theorem of linear control systems [28].

As in (11), the frequency response of $G_P(s)$ and $G_Q(s)$ at ω_o is obtained:

$$\underbrace{A_P e^{j\phi_P}}_{G_P(j\omega_o)} = \underbrace{A_H e^{j\phi_H}}_{H(j\omega_o)} \cdot K_P \cdot \underbrace{A_{CP} e^{j\phi_{CP}}}_{C_P(j\omega_o)} \cdot \underbrace{A_{PP} e^{j\phi_{PP}}}_{P_P(j\omega_o)}, \tag{13}$$

$$\underbrace{A_Q e^{j\phi_Q}}_{G_Q(j\omega_o)} = \underbrace{A_H e^{j\phi_H}}_{H(j\omega_o)} \cdot K_Q \cdot \underbrace{A_{CQ} e^{j\phi_{CQ}}}_{C_Q(j\omega_o)} \cdot \underbrace{A_{PQ} e^{j\phi_{PQ}}}_{P_Q(j\omega_o)}, \tag{14}$$

where subscripts CP and CQ refer to the compensators, while PP and PQ refer to the active and reactive power plants, respectively.

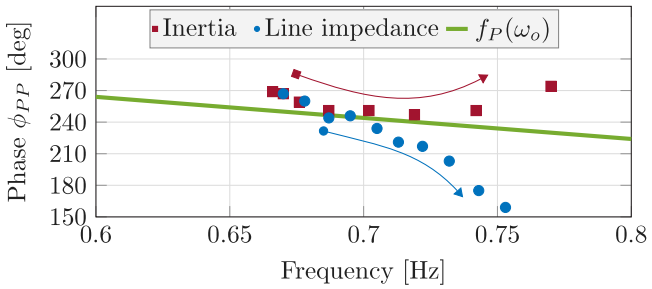

Fig. 5. Phase angle that needs to be compensated by the active-power POD (ϕ_{CP}) when the oscillation frequency changes (ω_o). Variation of (squares) inertia and (circles) line impedance values. (green) Line representing $f_P(\omega_o)$.

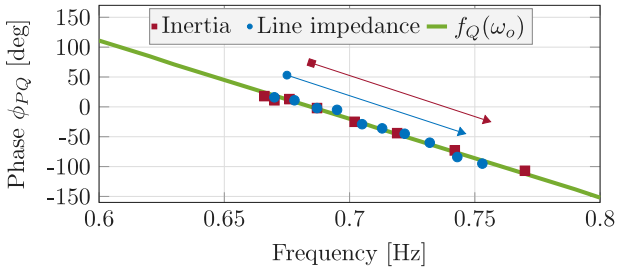

Fig. 6. Phase angle that needs to be compensated by the reactive-power POD (ϕ_{PQ}) when the oscillation frequency (ω_o) changes. Variation of (squares) inertia and (circles) line impedance values. (green) Line representing $f_Q(\omega_o)$.

3.4. Controller limits

Recalling that p^r and q^r are the active and reactive powers requested by the operator, the active and reactive power limits of the CIG can be calculated as follows:

$$p^l = k \cdot p^r, \tag{15}$$

$$q^l = \sqrt{S_n^2 - (p^l + p^r)^2} - q^r, \tag{16}$$

where $k \in [0, 1)$ is a predefined active-power margin available from the primary source to provide damping services. In this section, the method to adapt the POD controller is described. First, an offline simulation is conducted and the adjustment characteristic is defined. Then, the procedure to update the POD controller parameters is introduced.

3.5. Controller gain

The controller proportional gains K_P and K_Q are designed following the two-step method. First, the system performance is analysed for different values of the proportional gain. This allows for determining the gain value for which the damping of the system reaches a maximum. Then, to determine the final value of the controller gains, the system performance is verified using transient analysis. This approach is a compromise between improving the controller damping performance and ensuring robustness for different operating points.

4. POD controller adjustment

The lead–lag design criteria obtained in (12) can be applied to (13) and (14). Then, the following results are obtained:

$$\phi_{CP} = -\phi_H - \phi_{PP}, \tag{17}$$

$$\phi_{CQ} = -\phi_H - \phi_{PQ}. \tag{18}$$

This result means the compensators would compensate for the phase of the plant plus the phase of the high-pass filter (i.e., the open-loop phase). The phase that needs to be compensated can be in the range ±180 degrees. However, the maximum phase shift introduced by one lead–lag is limited to ±90 degrees. Therefore, the compensator is formed as a linear connection of two identical lead–lag compensators. This can be defined as:

$$n_p = n_q = 2. \tag{19}$$

The design of the gain of the compensator is simpler compared to the phase. Here, only the gain introduced by the high-pass filter is compensated. Then:

$$A_{CP} = A_{CQ} = 1/A_H. \tag{20}$$

With these specifications selected, the lead–lag parameters are calculated by using standard formulas [29].

4.1. Off-line analysis

4.1.1. Network reconfiguration aspects

In [30], it was found that changes in the impedance of the tie-line between areas have high impact on the frequency of the inter-area oscillation. This scenario happens when one line is disconnected after a fault. Another aspect that affects the frequency of the oscillation is variations in the system inertia. This scenario typically takes place when available renewable sources replace conventional generators in the generation mix that are then disconnected. Furthermore, the network reconfiguration causes the change in the POD controller plant, modifying the plant phase at oscillation frequency. Thus, the POD controller settings become inaccurate, deteriorating the damping performance. The impact of the network reconfiguration on the plant phase is addressed in following sections.

4.1.2. Analysis of active and reactive power dynamics

The aim of this section is to find the relationships between the oscillation frequency (ω_o) and the phases that will be addressed by the lead–lag filters (ϕ_{PP} and ϕ_{PQ}), within the frequency range of interest [31]. Changes in the interconnecting lines (l_1, l_2, and l_3 in Fig. 1) and reductions in the inertia of generators will be applied. For each modification in the system topology, the following steps need to be taken:

1. First, the network model is modified. Then, a three-phase fault is applied and cleared in the area formed by generators G_3 and G_4, at point F in Fig. 1. The system response includes the inter-area oscillation, in which the frequency of the oscillation should be detected. For that purpose, the zoom-FFT algorithm is used [32].
2. Then, the challenge is to find the angle to be compensated, and for that purpose the phase of the plant at ω_o (ϕ_{PP} and ϕ_{PQ}) should be calculated. The system is perturbed by using the CIG power references, depicted as points P and Q in Fig. 1. The disturbance signal is a sinusoidal of frequency ω_o that is applied in the active and reactive power references, consequently. When the simulation reaches steady-state, the angle between the sinusoidal disturbance input and the output is measured, thus obtaining ϕ_{PP} and ϕ_{PQ} (in two separate simulations). This process is programmed in a script so it does not require manual actions.

Figs. 5 and 6 show the estimated phases for the aforementioned network changes. Both phases mainly decrease when the impedance of the tie-line increases (circles) and when the system inertia decreases (squares). In Fig. 6, the linear relationship between ϕ_{PQ} and ω_o is clear. There is also a relation between ϕ_{PP} and ω_o, although it is not as clear as for ϕ_{QP}. It can be seen that the modification in tie-line resulted in a linearly descending angle ϕ_{PP}, while modification in the generators inertia resulted in a non-linear relation between ϕ_{PP} and ω_o.

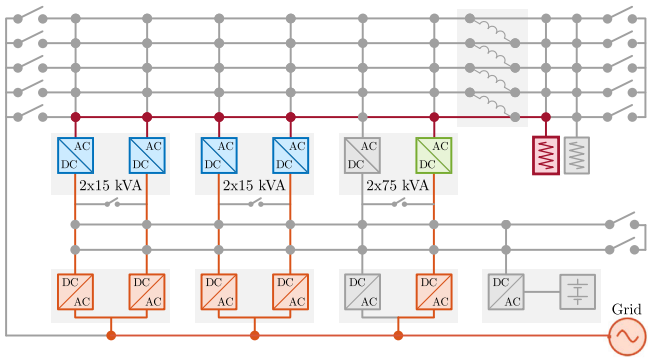

Fig. 7. Electric diagram of the laboratory facilities. (green) Grid emulator and (blue) VSCs used as CIGs.

4.1.3. Fitting the phase-frequency functions

The results obtained in the previous section are used here to fit $f_P(\omega_o)$ and $f_Q(\omega_o)$. For simplicity, a linear function has been considered here, although different curves may be used here:

$$f_P(\omega_o) = m_P \cdot \omega_o + s_P, \tag{21}$$

$$f_Q(\omega_o) = m_Q \cdot \omega_o + s_Q, \tag{22}$$

where m and s refer to the slope and constant values of the straight line. For fitting the values, any method can be used (e.g., minimum squares). The resulting functions are depicted in Figs. 5 and 6, in green.

4.2. Real-time operation

The calculation of functions $f_P(\omega_o)$ and $f_Q(\omega_o)$ require only basic mathematical operations. Therefore, these functions can be simply implemented in local controllers. The practical implementation is shown in Fig. 2(b). Firstly, the frequency of the oscillation is estimated by using the zoom-FFT algorithm. This algorithm was selected for its precision and low computational requirements, which makes it suitable for real-time implementations. Nonetheless, the oscillation frequency can be estimated using other estimation techniques. Also, such information could be extracted from ambient data, by analysing the frequency content of measured currents and voltages. Furthermore, the proposed implementation is suitable for systems with oscillations in the low-frequency range. If the system faces oscillations at higher frequencies, the proposed method could be connected with methods used for detecting subsynchronous oscillations [33].

Once ω_o is estimated, it is used to calculate compensation angles, ϕ_{CP} and ϕ_{CQ}. Finally, the parameters of the lead–lag compensators are adjusted to achieve new compensation angles following the procedure described in Section 3.3. It should be noted that the phase introduced by additional elements in the loop should also be compensated by the lead–lag compensators (e.g., if additional low-pass filters are applied). Also, the adjustment of the control parameters leads to a sudden increase or decrease in the power references. However, the limiters p^l and q^l would ensure that the final command signals do not exceed the allowed limits.

5. Experimental validation

5.1. Experimental setup description

The proposed POD controller performance was experimentally validated in a laboratory [34]. Fig. 7 shows a single-line diagram of the laboratory facilities. The nominal network voltage was 400 V and the nominal frequency 50 Hz. The two-area power system depicted in Fig. 1(a) was emulated by using one 75 kVA VSC. This converter includes fast internal controllers so it can readily emulate grids [34]. The CIGs were emulated by using four 15 kVA VSCs connected to the grid via their LCL filters. Each of these CIGs included an adaptive POD controller. The CIGs did not have communication links between them. All the CIGs were connected to the same busbar (the POC), which is the output of the grid emulator. The dc sides of all converters were maintained constant at 680V by using uncontrolled rectifiers. The switching and sampling frequencies for the 75 kVA and 15 kVA VSCs were 8 kHz and 10 kHz, respectively (see [34] for more details). The laboratory measurements were scaled up so that 1 kVA in the laboratory was seen as 75 MVA in the emulated power system. For the internal current controllers of the CIGs, the settling time was set to 5 ms and the overshoot to 10 %. PLLs used in each CIG for the synchronisation were designed assuming a settling time of 80 ms and 10 % overshoot. The zoom-FFT algorithm was adjusted to operate in the frequency range between 0.1 and 2 Hz.

5.2. Experimental results

5.2.1. Active power, reactive power and combined POD controller

In this section, the proposed POD controller was tested without the adjustment mechanism applied and was designed following the procedure described in Section 3. For this scenario, the oscillation frequency of the system was 0.64 Hz. The frequency responses of $P_P(j\omega_o)$ and $P_Q(j\omega_o)$ were measured by perturbing the system at f_o. Then, from (17) and (18) the compensation angles were calculated. The active and reactive power limits (p^d and q^d) were equal and set to 0.12 pu. Equal limits were selected in order to compare the effectiveness of active and reactive power. Then, the controller proportional gains were calculated so that they do not saturate when a transient takes place. More advanced criteria can be used for the design of the gains, but this is not explored here.

Fig. 8(a) shows the transient response of the grid frequency for three test cases. In (blue) only active power is used, in (red) only reactive power, and in (green) both powers are used simultaneously. In addition, the injected active and reactive power during the transient from one CIG are shown in Fig. 8(b) and Fig. 8(c), respectively. In all three cases, the system damping improved compared to the case without the POD controller (in grey). It can be seen that the best damping was achieved for the case in which both powers active and reactive are used. This can be verified in Fig. 9, where the most critical eigenvalues (those related to the inter-area oscillation) obtained in the experimental verification are shown. These eigenvalues were identified by applying a pseudo-random binary signal (PRBS) to the command of the power references and then by estimating the system model and its eigenvalues. In (grey), the critical eigenvalue without any POD controller is shown, in (blue) with the POD controller only acting with active power, in (green) only with reactive power, and in (red) with both power components. Without the POD controller, the critical eigenvalues had a natural frequency of 4.05 rad/s and a damping factor of 0.016. For the POD controllers based only on active and reactive power, the eigenvalues clearly move away from instability. However, the combined action of both power components gave the best results, and a damping factor of 0.067 was obtained.

5.2.2. Network reconfiguration

In order to validate the benefits of the proposed adaptive mechanism, a representative scenario in which an inter-area oscillation appears was selected. In this scenario, the inertia constant of generators G_1 and G_3 was reduced by 10 %, while the reduction was 15 % for generators G_2 and G_4 (see Fig. 1). Furthermore, the proportional gain of PSS in G_2 was reduced by 33 % in order to make the system marginally stable after the disconnection of a line. The main objective of this change was to demonstrate the benefits of the proposed control technique. This scenario can be explained using Fig. 10(a). In this scenario, the system was initially stable and the CIG-based power plant was designed to provide the maximum damping by using both active

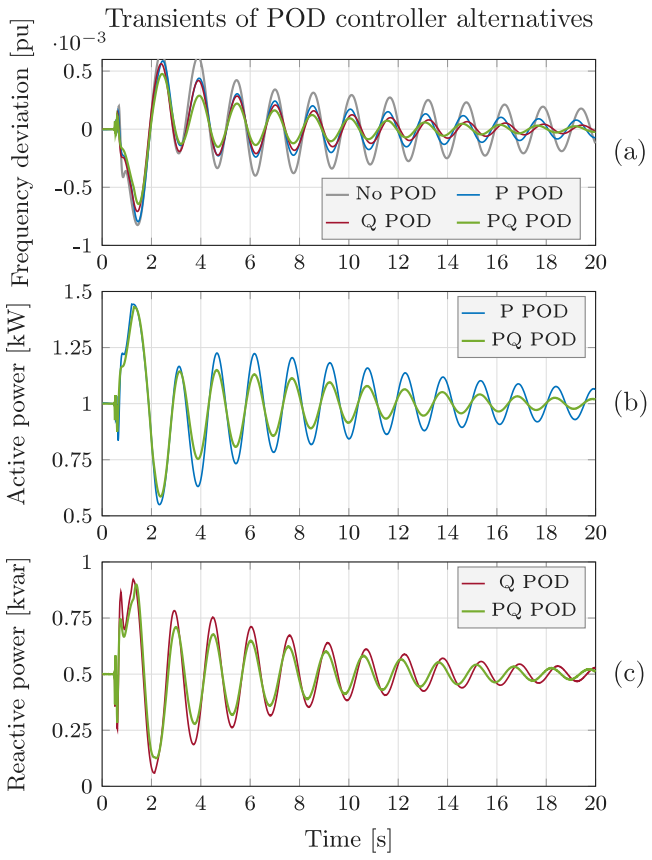

Fig. 8. Laboratory results. (a) Frequency deviation, (b) active and (c) reactive power injected by the CIGs. The meaning of colours is marked in the legends.

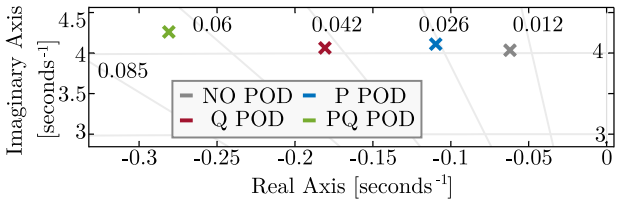

Fig. 9. Critical eigenvalue identified in the laboratory for the POD controller options. (grey) No POD controller, (blue) only active power, (green) only reactive power and (red) active and reactive power.

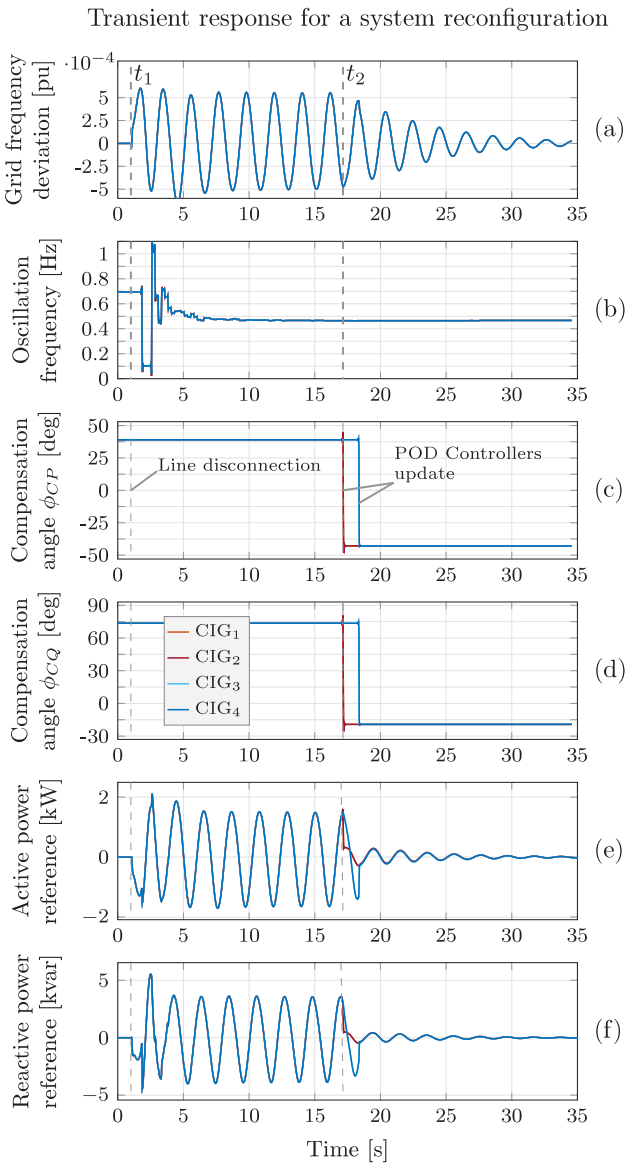

Fig. 10. Transient response of (a) the grid frequency, (b) active and (c) reactive power when one line is disconnected and the adaptive mechanism is applied. (d) Compensation angles calculated in real time. (e) Active and (f) reactive power references.

and reactive power injection. Eventually, tie-line l_3 (see Fig. 1) was disconnected at $t_1 = 1$ s and then the system was very close to instability. This happens because the system dynamics changed significantly and the original POD controller cannot guarantee adequate system damping. This change in the system topology also caused a change in the oscillation frequency.

During the first three oscillation periods the FFT algorithm was estimating the oscillation frequency, and the new value was determined after approximately 6 s (Fig. 10(b)). Then, the compensation angles updated according to $f_P(\omega_o)$ and $f_Q(\omega_o)$ (instant t_2). These curves were calculated according to the realistic elements included in the laboratory (additional delays and filters, etc.) so they have differences compared to those shown in Figs. 5 and 6. It can be observed that the angles of all the CIGs were not updated at the same time. This happens because they are operated independently and, therefore, their controllers are not synchronised (Fig. 10 (c, d)). After instant t_2, the transient response shows that the sustained oscillation was clearly damped due the action of the adaptation mechanism. The adjustment can also be seen in the active and reactive power references, in Fig. 10(e) and (f), respectively. In both references, the adjusted parameters resulted in a sudden decrease in the signal amplitude. Fig. 11 shows the system eigenvalues for the aforementioned scenario. In (light blue), the system damping before the event is shown. It can be seen that the system was well damped. Then, in (dark blue), the line was disconnected and the mode moved towards the imaginary axis, while the oscillation frequency clearly decreased. Finally, in (red), when the controller was updated, the system became well damped again. For completeness, in (yellow, green) the system eigenvalues in the original and final states are shown, but without any POD controller. It can be seen that in these cases the system was not well damped.

5.2.3. POD adjustment robustness

To explore the robustness of the proposed method with respect to the selection of functions $f_P(\omega_o)$ and $f_Q(\omega_o)$, the values of the slopes were intentionally modified. Fig. 12 shows the damping of the most critical eigenvalue for the variations of the slope, $\Delta m = m/m_s$ (the same for P and Q), where m_s was the original slope. It can be seen that for

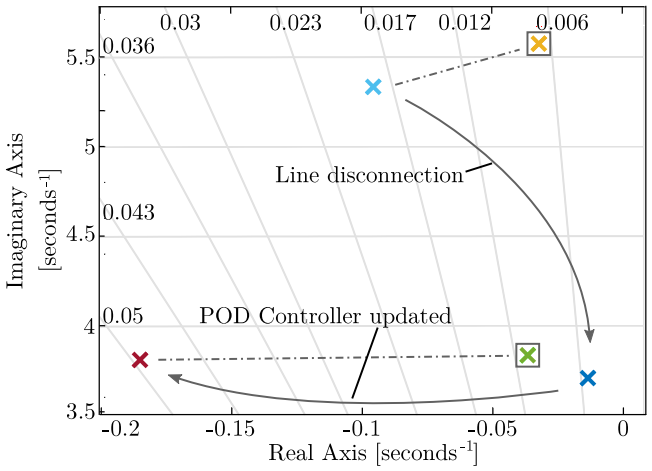

Fig. 11. System eigenvalues for the system reconfiguration. (light blue) Initial state, (dark blue) after the line disconnection and (red) once the controller is adapted. (yellow, green) Initial and final states without POD controller.

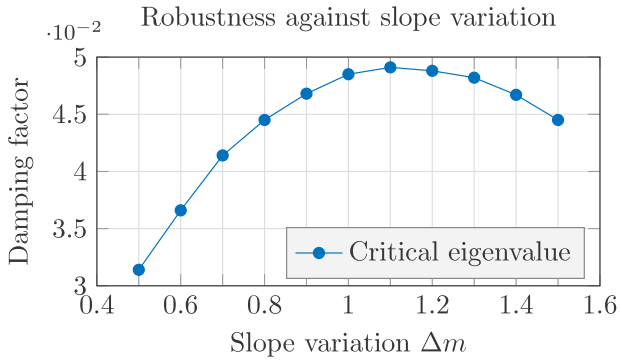

Fig. 12. Laboratory measurements. Damping of the most critical eigenvalue when the slope of the adjustment characteristic is modified.

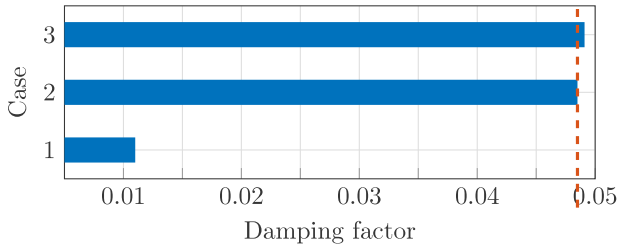

Fig. 13. Damping of the most critical mode (1) without POD controller, POD controller design (2) with the proposed method, and (3) for the maximum damping.

variations between 1.5 and 0.5, the damping still remained larger than 0.04. However, the damping rapidly decreased if Δm was lower than 0.5. The effect of the slope and the selection of the curve is relevant, and its selection greatly depends on the system topology. Therefore, exploring this for different power system topologies is of interest for further research.

5.3. Comparison with other methods for POD controller design

In the literature, the POD controllers are often designed with a focus on maximising the damping factor of the critical mode. To do so, either a single-objective [35] or multi-objective [36] optimisation functions can be defined. These objectives are defined as minimising the mode with the largest damping factor value [37] or maximising the

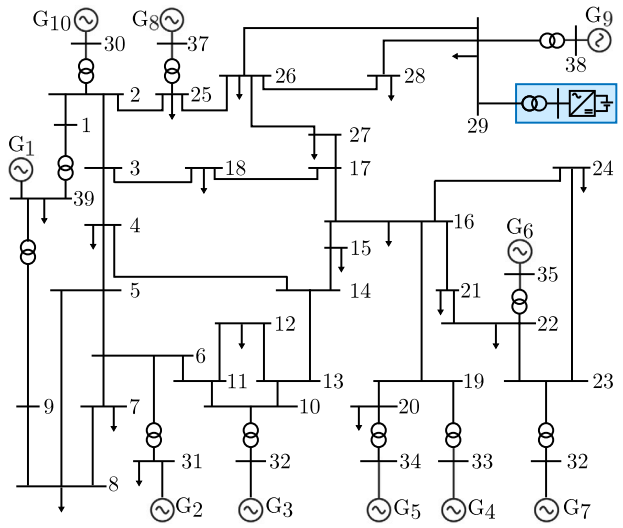

Fig. 14. Single-line diagram of IEEE 39-Bus with (blue) additional CIG.

mode with the lowest damping ratio [38]. Also, these objectives can be merged to define the expected values for both the damping ratio and factors of dominant modes [39]. Fig. 13 shows the damping factor of the critical mode for three cases. *Case 1* represents the case without the POD controller, while the POD controller is included in *Case 2* and *Case 3*. In *Case 2*, the POD controller was designed with the procedure presented in this work. Then, in *Case 3*, the controller was designed for the maximum damping factor. It can be seen that if the POD controller compensates the open-loop phase shift the achieved damping factor is not at the maximum. However, it is very close to it while the analytical solution is easy to obtain.

6. Analysis on larger system

Fig. 14 shows the single-line diagram of a modified IEEE 39-Bus system. The first modification is the reduction of the proportional gains of all PSS in the system by 30 %. The second modification is the connection of the CIG to the Bus-29 via a step-up transformer. Then, the system was observed from the CIG active and reactive power references for different modifications. These modifications included changes in the line impedance, inertia of generators, as well as disconnection of one line at a time. During this procedure the changes in both oscillation frequency (ω_o) and plant phases (ϕ_{CP} and ϕ_{CQ}) were examined.

Fig. 15 and Fig. 16 show results of the analysis for the active and reactive power loops, respectively. Since the power system included several modes, the frequency responses included three peaks around 0.4, 0.8 and 1.1 Hz. A similar trend can be seen for both (red) increase in line impedance and (blue) decrease in the inertia of generators. For both sets of modifications, the phase to be compensated decreased as the frequency of oscillations increases. Furthermore, the changes in (yellow) network topology have resulted in a wider range of changes in ω_o. Nonetheless, these modifications result in the same trend for compensation angles in both active and reactive power loops.

7. Conclusion

In this paper, a POD controller for CIGs that uses both active and reactive power has been presented. This controller maximises the capability of CIGs to damp oscillations and offers parameter adaptation when a change of the network dynamics is detected. Possible network changes are analysed off-line and the value of each oscillation frequency is linked then with the angle that needs to be compensated by

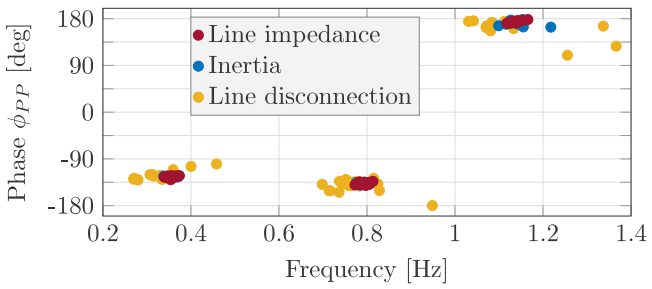

Fig. 15. Analysis for IEEE 39 Bus network: Phase angle that needs to be compensated by the active-power POD controller (ϕ_{CP}) when the oscillation frequency (ω_o) changes.

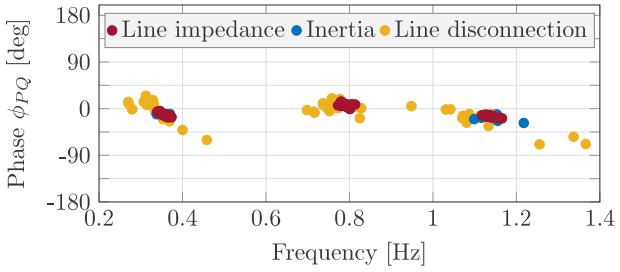

Fig. 16. Analysis for IEEE 39 Bus network: Phase angle that needs to be compensated by the active-power POD controller (ϕ_{CQ}) when the oscillation frequency (ω_o) changes.

the active and reactive power controllers. The information from the off-line analysis is then applied in real-time to adapt the POD controller. Theoretical derivations were validated using the laboratory setup, in which four 15 kVA CIGs were connected to a 75 kVA grid emulator that reproduced the dynamics of a two-area power system. Furthermore, a theoretical analysis was conducted for the IEEE 39-Bus system, showing a similar relationship between the oscillation frequency and angle that needs to be compensated.

Results have shown that each oscillation frequency is linked with an angle that can be compensated by using active and reactive power controllers. These links may vary depending on the elements that created the change of topology or network parameters (line disconnection or inertia variation), and the most relevant cases must be included in the offline analysis. Also, theoretical results have shown that the best strategy to damp oscillations is that each POD controller (for active and reactive powers) compensates for the phase lag of its open-loop transfer function. Experimental results were in good agreement with the theoretical studies. The main question regarding this method would be how would it perform in different systems, since the relation between compensation angles and oscillation frequency greatly depends on the system topology. This is of interest for further study and research.

CRediT authorship contribution statement

Njegos Jankovic: Conceptualization, Methodology, Software, Writing – original draft. **Javier Roldan-Perez:** Validation, Visualization, Software, Writing – original draft. **Milan Prodanovic:** Supervision, Writing – review & editing. **Jon Are Suul:** Supervision, Writing – review & editing. **Salvatore D'Arco:** Supervision, Writing – review & editing. **Luis Rouco Rodriguez:** Supervision, Writing – review & editing.

Declaration of competing interest

The authors declare that they have no known competing financial interests or personal relationships that could have appeared to influence the work reported in this paper.

Data availability

No data was used for the research described in the article.

References

[1] Kundur P, Balu N, Lauby M. Power system stability and control. EPRI power system engineering series, McGraw-Hill; 1994.
[2] Padiyar K. Power system dynamics stability and control. BS Publications; 2008.
[3] Quintero J, Vittal V, Heydt GT, Zhang H. The impact of increased penetration of converter control-based generators on power system modes of oscillation. IEEE Trans Power Syst 2014;29(5):2248–56.
[4] European Commission. Commission regulation establishing a network code on requirements for grid connection of generators. 2016.
[5] Larsen EV, Swann DA. Applying power system stabilizers part I: General concepts. IEEE Trans Power Appar Syst 1981;PAS-100(6):3017–24.
[6] Liu Y, Zhu L, Zhan L, Gracia JR, King Jr T, Liu Y. Active power control of solar PV generation for large interconnection frequency regulation and oscillation damping. Int J Energy Res 2016;40(3):353–61.
[7] Bhukya J, Mahajan V. Optimization of controllers parameters for damping local area oscillation to enhance the stability of an interconnected system with wind farm. Int J Electr Power Energy Syst 2020;119:105877.
[8] Silva-Saravia H, Pulgar-Painemal H, Tolbert LM, Schoenwald DA, Ju W. Enabling utility-scale solar PV plants for electromechanical oscillation damping. IEEE Trans Sustain Energy 2021;12(1):138–47.
[9] Edrah M, Lo KL, Anaya-Lara O. Reactive power control of DFIG wind turbines for power oscillation damping under a wide range of operating conditions. IET GTD 2016;10(15):3777–85.
[10] Knuppel T, Kumar S, Thuring P, Stottrup M, Friman J. Towards a reactive power oscillation damping controller for wind power plant based on full converter wind turbines. In: 2012 IEEE PES GM. 2012, p. 1–8.
[11] Basu M, Mahindara VR, Kim J, Nelms RM, Muljadi E. Comparison of active and reactive power oscillation damping with PV plants. IEEE Trans Ind Appl 2021;57(3):2178–86.
[12] Varma RK, Maleki H. PV solar system control as STATCOM (PV-STATCOM) for power oscillation damping. IEEE Trans Sustain Energy 2019;10(4):1793–803.
[13] Li M, Xiong L, Chai H, Xiu L, Hao J. Mechanism of PV generation system damping electromechanical oscillations. IEEE Access 2020;8:135853–65.
[14] Rimorov D, Kamwa I, Joos G. Coordinated design of active and reactive power modulation auxiliary loops of wind turbine generators for oscillation damping in power systems. In: 2015 IEEE PES GM. 2015, p. 1–5.
[15] Guo J, Wang X, Ooi B-T. Online model-free estimation of the dynamic system model for a power system with renewables in ambient conditions. IEEE Access 2020;8:96878–87.
[16] Chaudhuri N, Domahidi A, Majumder R, Chaudhuri B, Korba P, Ray S, et al. Wide-area power oscillation damping control in Nordic equivalent system. IET GTD 2010;4:1139–50.
[17] Ma J, Wang T, Wang S, Gao X, Zhu X, Wang Z, et al. Application of dual youla parameterization based adaptive wide-area damping control for power system oscillations. IEEE Trans Power Syst 2014;29:1602–10.
[18] Leon AE, Solsona JA. Power oscillation damping improvement by adding multiple wind farms to wide-area coordinating controls. IEEE Trans Power Syst 2014;29(3):1356–64.
[19] Tang K, Venayagamoorthy GK. Adaptive inter-area oscillation damping controller for multi-machine power systems. Electr Power Syst Res 2016;134:105–13.
[20] Abdelsalam HA, Ahmed AA, Diab AAZ. Trajectory sensitivity analysis-based systematic Q-matrix of DFIG with LQR auxiliary voltage and power compensation for oscillation damping. Int J Electr Power Energy Syst 2022;135:107575.
[21] Beza M, Bongiorno M. An adaptive power oscillation damping controller by STATCOM with energy storage. IEEE Trans Power Syst 2015;30(1):484–93.
[22] Chau TK, Yu SS, Fernando T, Iu HH-C, Small M. A load-forecasting-based adaptive parameter optimization strategy of STATCOM using ANNs for enhancement of LFOD in power systems. IEEE Trans Ind Inform 2018;14(6):2463–72.
[23] Chaiyatham T, Ngamroo I. Improvement of power system transient stability by PV farm with fuzzy gain scheduling of PID controller. IEEE Syst J 2017;11(3):1684–91.
[24] Liao K, Xu Y, Zhou H. A robust damping controller for DFIG based on variable-gain sliding mode and Kalman filter disturbance observer. Int J Electr Power Energy Syst 2019;107:569–76.
[25] Yazdani A, Iravani R. Grid-imposed frequency VSC system: Control in -frame. In: Voltage-sourced converters in power systems: Modeling, control, and applications. John Wiley and Sons, Ltd; 2010, p. 160–203.
[26] Zhao J, Huang M, Yan H, Tse CK, Zha X. Nonlinear and transient stability analysis of phase-locked loops in grid-connected converters. IEEE Trans Power Electron 2021;36(1):1018–29.
[27] MATLAB. version 9.7.0 (R2019b). 2019, The MathWorks Inc. Natick, Massachusetts.
[28] Ogata K. Modern control engineering. Prentice hall; 2010.

[29] Jankovic N, Roldan-Perez J, Prodanovic M. Power oscillation damping using converter-interfaced generators under constrained active and reactive powers. In: IEEE ISGT Europe. 2021, p. 1–8.
[30] Klein M, Rogers G, Kundur P. A fundamental study of inter-area oscillations in power systems. IEEE Trans Power Syst 1991;6(3):914–21.
[31] Rogers G. Power system oscillations. Springer Science & Business Media; 2012.
[32] Lyons RG. Understanding digital signal processing, 3/E. Pearson Education India; 2004.
[33] Shair J, Xie X, Yang J, Li J, Li H. Adaptive damping control of subsynchronous oscillation in DFIG-based wind farms connected to series-compensated network. IEEE Trans Power Deliv 2022;37(2):1036–49.
[34] Roldán-Pérez J, Morán-Rio DP, Moutevelis D, Rodríguez-Ortega P, Jankovic N, Ebrahim Zarei M, et al. Emulation of complex grid scenarios by using power hardware in the loop (PHIL) techniques. In: 2021 IEEE Toronto IECON. 2021, p. 1–6.
[35] Khadanga RK, Satapathy JK. Time delay approach for PSS and SSSC based coordinated controller design using hybrid PSO–GSA algorithm. Int J Electr Power Energy Syst 2015;71:262–73.
[36] Ali E. Optimization of power system stabilizers using BAT search algorithm. Int J Electr Power Energy Syst 2014;61:683–90.
[37] Eslami M, Shareef H, Taha MR, Khajehzadeh M. Adaptive particle swarm optimization for simultaneous design of UPFC damping controllers. Int J Electr Power Energy Syst 2014;57:116–28.
[38] Mary Linda M, Kesavan Nair N. A new-fangled adaptive mutation breeder genetic optimization of global multi-machine power system stabilizer. Int J Electr Power Energy Syst 2013;44(1):249–58.
[39] Rahmatian M, Seyedtabaii S. Multi-machine optimal power system stabilizers design based on system stability and nonlinearity indices using Hyper-Spherical Search method. Int J Electr Power Energy Syst 2019;105:729–40.